January 2016

Chimera states in a Hodgkin-Huxley model of thermally sensitive neurons

Tera Glaze

Scott Lewis

Sonya Bahar
University of Missouri

Recommended Citation

Glaze, Tera; Lewis, Scott; and Bahar, Sonya, "Chimera states in a Hodgkin-Huxley model of thermally sensitive neurons" (2016). *Physics Faculty Works*. 10.
DOI: https://doi.org/10.1063/1.4961122
Available at: https://irl.umsl.edu/physics-faculty/10

Chimera states in a Hodgkin-Huxley model of thermally sensitive neurons

Cite as: Chaos **26**, 083119 (2016); https://doi.org/10.1063/1.4961122
Submitted: 29 February 2016 . Accepted: 02 August 2016 . Published Online: 23 August 2016

Tera A. Glaze, Scott Lewis, and Sonya Bahar

Chimera states in a Hodgkin-Huxley model of thermally sensitive neurons

Tera A. Glaze,[1] Scott Lewis,[2] and Sonya Bahar[1,a)]
[1]*Department of Physics & Astronomy and Center for Neurodynamics, University of Missouri at St. Louis, St. Louis, Missouri 63121, USA*
[2]*Department of Biology, University of Missouri at St. Louis, St. Louis, Missouri 63121, USA*

(Received 29 February 2016; accepted 2 August 2016; published online 23 August 2016)

Chimera states occur when identically coupled groups of nonlinear oscillators exhibit radically different dynamics, with one group exhibiting synchronized oscillations and the other desynchronized behavior. This dynamical phenomenon has recently been studied in computational models and demonstrated experimentally in mechanical, optical, and chemical systems. The theoretical basis of these states is currently under active investigation. Chimera behavior is of particular relevance in the context of neural synchronization, given the phenomenon of unihemispheric sleep and the recent observation of asymmetric sleep in human patients with sleep apnea. The similarity of neural chimera states to neural "bump" states, which have been suggested as a model for working memory and visual orientation tuning in the cortex, adds to their interest as objects of study. Chimera states have been demonstrated in the FitzHugh-Nagumo model of excitable cells and in the Hindmarsh-Rose neural model. Here, we demonstrate chimera states and chimera-like behaviors in a Hodgkin-Huxley-type model of thermally sensitive neurons both in a system with Abrams-Strogatz (mean field) coupling and in a system with Kuramoto (distance-dependent) coupling. We map the regions of parameter space for which chimera behavior occurs in each of the two coupling schemes. *Published by AIP Publishing.*
[http://dx.doi.org/10.1063/1.4961122]

The chimera state is a dynamical phenomenon that has been the subject of significant recent interest. This state occurs when two groups of identical oscillators are coupled to one another but exhibit drastically different behaviors, in which one group of oscillators is synchronized and the other is not. Chimera states have been observed experimentally in various types of systems, such as mechanical (Martens *et al.*, 2013), optical (Hagerstrom *et al.*, 2012), and chemical (Tinsley *et al.*, 2012). Given the importance of synchronization in the brain for both health and disease, investigation of chimera states in neural models is of particular interest. It has been speculated that chimera states might serve as a model for the differences in activity between brain hemispheres during unihemispheric sleep. This phenomenon, in which hemispheres alternately exhibit sleep-like behavior while the other hemisphere stays "awake," has been observed in aquatic mammals (Mukhametov, 1984), ducks (Rattenborg *et al.*, 1999), and lizards (Mathews *et al.*, 2006). Recent observations of asymmetric brain activity in human sleep apnea patients (Rial *et al.*, 2013) suggest that the study of neural chimera states may have clinical relevance as well. Chimera states in neural systems are also of particular relevance for their similarity to "bump" states (Laing, 2001), which have been suggested as a possible model for various forms of cortical information processing such as visual orientation tuning and working memory. Here, we demonstrate chimera states in a Hodgkin-Huxley-type model of temperature sensitive neurons for two different coupling schemes.

I. INTRODUCTION

The recent discovery of *chimera states* in networks of coupled oscillators, in which groups of identically coupled oscillators exhibit qualitatively different dynamical behaviors, has generated great interest not only theoretically but also for its potential applications. Chimera behavior was first observed in a ring of simple oscillators (Kuramoto and Battogtokh, 2002). This behavior was also studied in the same system by Abrams and Strogatz (2004), with the substitution of a different kernel in the integral expression governing the rate of change of each oscillator's phase, in order to allow for an analytical solution of the model. Chimera behavior was also identified in a new model with a different coupling scheme (Abrams-Strogatz coupling), developed specifically for the investigation of chimera behavior, by Abrams *et al.* (2008).

In Kuramoto coupling, a ring of identically, non-locally coupled oscillators can—for certain parameter ranges—spontaneously separate into groups, one of which exhibits synchronous oscillations and the other of which exhibits unsynchronized behavior. In contrast, Abrams-Strogatz coupling uses two globally coupled groups of oscillators. Each group is also weakly coupled to the mean field of the other group. For certain parameter ranges and coupling constants, one of the two groups exhibits synchronous behavior, and the other remains unsynchronized. In other cases, *phase-cluster* states have been observed, where the two groups of

a)Author to whom correspondence should be addressed. Electronic mail: bahars@umsl.edu.

oscillators exhibit different types of oscillatory behaviors (Tinsley *et al.*, 2012).

Since the first observation of chimera behavior, the phenomenon has been investigated both theoretically and experimentally. The underlying dynamics of the phenomenon are not yet fully understood, and it has been suggested that chimera states may be chaotic transients (Wolfrum and Omel'chenko, 2011). Chimera behavior has been investigated experimentally in mechanical (Martens *et al.*, 2013) and optical (Hagerstrom *et al.*, 2012) systems as well as in systems of chemical oscillators (Tinsley *et al.*, 2012; Wickramasinghe and Kiss, 2013; and Nkomo *et al.*, 2013).

It should come as no surprise that a particular area of interest lies in the application of chimera behavior to neural systems. Coupling in neural systems has long been a subject of intense investigation due to the role it may play in pathological states such as seizures (Isomura *et al.*, 2008 and Bartolomei *et al.*, 2013), Parkinson's disease (Popovych *et al.*, 2005; Tass *et al.*, 2012; and Adamchic *et al.*, 2014), as well as its possible role in mediating states of attention (Fries *et al.*, 2001) and possibly consciousness itself (Tononi and Koch, 2008).

In the context of chimera behavior, a particular point of interest is the phenomenon of unihemispheric sleep, in which animals are able to "decouple" their brain hemispheres in order to sleep while in the ocean (Lyamin *et al.*, 2008), at rest (Rattenborg *et al.*, 1999), or on the wing (Rattenborg, 2006). This enables the animals to continue swimming or flying, while observing their environment and navigating, and alternately resting part of their neural systems. There is even evidence that seals use bihemispheric sleep when on land and revert to unihemispheric sleep when at sea (Mukhametov, 1984). Ducks use unihemispheric sleep while resting in groups, specifically at the outer edges of the group, where the danger of predation is greatest (Rattenborg *et al.*, 1999). It is speculated that some species of lizard may utilize unihemispheric sleep while under duress from a predator (Mathews *et al.*, 2006).

Unihemispheric sleep has recently become a subject of significant interest in the context of human health, as a result of the recent observation of asymmetric sleep in human subjects with sleep apnea by Rial *et al.* (2013). A scale has even been developed which represents the relationship between hemisphere asymmetry and severity of sleep apnea, called the "interhemispheric synchrony index" (Abeyratne *et al.*, 2010). Tamaki *et al.* (2016) observed interhemispheric asynchrony in humans during their first night sleeping in a novel environment.

Given the relevance of chimera states for neural behavior, several studies of this phenomenon in dynamical models of excitable cells have been undertaken in recent years. Omelchenko *et al.* (2013) observed chimera states in a network of coupled FitzHugh-Nagumo oscillators, a nonlinear ordinary differential equation model that has been used extensively to model various types of excitable cells, such as cardiac myocytes. Hizanidis *et al.* (2014) observed chimera states in a simulated network of neurons using the Hindmarsh-Rose model, a three-variable neural model that, while not incorporating the more realistic dynamics of a Hodgkin-Huxley-type model, does allow for realistic behavior such as burst-firing. (Burst-firing refers to temporally clustered action potentials, with a minimal recovery period between the action potentials within a burst, and longer intervals between successive bursts.)

In the present paper, we demonstrate chimera states using a network of neurons described by the Huber-Braun model (Braun *et al.*, 1998; Huber *et al.*, 2000; and Braun *et al.*, 2000). This Hodgkin-Huxley-based model was developed explicitly to emulate the oscillatory dynamics of mammalian facial cold receptors. Its unique bifurcation behavior includes both period-doubling and period-adding bifurcations as a temperature parameter is varied; the two bifurcation cascades collide in a homoclinic crisis (Feudel *et al.*, 2000). This is a dynamically rich, biologically realistic system in which to investigate chimera states. It is more realistic than the FitzHugh Nagumo, integrate-and fire, and Hindmarsh-Rose models, in that it exhibits a realistic set of bursting behaviors. It is a Hodgkin-Huxley-based model that incorporates sodium and potassium channels as well as slower calcium and calcium-dependent potassium channels and a chloride leak current, and has parameter values tuned to biologically realistic values which reproduce observed experimental behavior of mammalian cold receptors. In what follows, we illustrate chimera behavior in this system using both Kuramoto coupling and Abrams-Strogatz coupling.

II. THE MODEL

The mathematical details of the Huber-Braun model have been presented elsewhere (see Braun *et al.*, 1998), but we review them here for completeness. As is typical in this type of neural model, the rate of change of the membrane potential of neuron i is expressed as the sum of voltage-dependent current terms

$$C_M \frac{dV_i}{dt} = -I_l - I_d - I_r - I_{sd} - I_{sr} + \varepsilon + c_i. \tag{1}$$

The factor C_M gives the membrane capacitance in μF/cm^2 and is set to unity. The first term, I_l, is a passive leak current presumed to be carried primarily by Cl^- ions and is given as

$$I_l = g_l(V_i - V_l), \tag{2}$$

where g_l is the maximum conductance for the channels mediating this current, and V_l is the current's reversal potential. I_d is a simplified Hodgkin-Huxley depolarizing (Na^+) current, and I_r is a repolarizing (K^+) current. The last two currents, I_{sd} and I_{sr}, describe slow depolarizing (Ca^{++}) and slow repolarizing (Ca^{++}-dependent K^+) currents, respectively. The currents I_d, I_r, and I_{sd} have the form

$$I_k = \rho g_k a_k (V_i - V_k), \tag{3}$$

with $k = d$, r, or sd, and where ρ is a temperature-dependent scaling factor defined as

$$\rho = 1.3^{(T-T_0)/10}, \tag{4}$$

TABLE I. Parameters used in Huber-Braun model.

g_d (mS/cm^2)	1.5
g_r (mS/cm^2)	2.0
g_{sd} (mS/cm^2)	0.25
g_{sr} (mS/cm^2)	0.4
g_l (mS/cm^2)	0.1
V_d (mV)	50
V_r (mV)	−90
V_{sd} (mV)	50
V_{sr} (mV)	−90
V_l (mV)	−60
τ_d (ms)	0.1
τ_r (ms)	2.0
τ_{sd} (ms)	10
τ_{sr} (ms)	20
s_d (mV^{-1})	0.25
s_r (mV^{-1})	0.25
s_{sd} (mV^{-1})	0.09
V_{0d} (mV)	−25
V_{0r} (mV)	−25
V_{0sd} (mV)	−40
η	0.012
k	0.17
D (A^2/s)	100

with $T_0 = 25^\circ$ C and $T = 30^\circ$ C, parameter values for which uncoupled neurons exhibit periodic firing of single action potentials. The model exhibits complex bifurcation behavior as the parameter T is varied, as discussed, for example, by Braun *et al.* (1998) and Feudel *et al.* (2000). This parameter is held constant in the present study.

V_k represents the reversal potential of current k, and g_k is the corresponding maximum conductance. The factor a_k represents an activation variable; by taking on values between 0 and 1, it characterizes the probability of channels opening to allow the flow of current I_k. It is given by

$$da_k/dt = \phi(a_{k,\infty} - a_k)/\tau_k. \tag{5}$$

Here, τ_k is a time constant, ϕ is another temperature-dependent scaling factor, given by

$$\phi = 3.0^{(T-T_0)/10}, \tag{6}$$

and $a_{k,\infty}$ is a voltage-dependent steady-state activation term

$$a_{k,\infty} = \{1 + \exp[-s_k(V_i - V_{0k})]\}^{-1}, \tag{7}$$

where s_k is a steepness parameter given in mV^{-1}, and V_{0k} is a half-activation constant. Finally, the fourth current, I_{sr}, is given as

$$I_{sr} = \rho g_{sr} a_{sr}(V_i - V_{sr}). \tag{8}$$

While this equation has the same structure as the other currents, the activation variable a_{sr} includes an explicit dependence on I_{sd} because the slow K^+ current I_{sr} is dependent on the Ca^{++} current I_{sd}. The activation variable is given as

$$da_{sr}/dt = \phi(-\eta I_{sd} - k a_{sr})/\tau_{sr}. \tag{9}$$

The term ε in Eq. (1) is a Gaussian white noise term implemented using a Box-Mueller algorithm (Fox *et al.*, 1988). The noise is delta-correlated, with zero mean and variance $2D$, where D is the noise intensity. This means that the noise term satisfies $\langle \varepsilon(t)\varepsilon(t')\rangle = 2D\delta(t-t')$ and $\langle \varepsilon(t)\rangle = 0$. The last term in (1), c_i, is a coupling term. This can be defined in various ways depending on the coupling scheme of interest and will be discussed in more detail below. Simulations are performed in custom-written MATLAB code, using Euler integration with a step size of 0.01 ms. In all simulations below, parameters are set to the physiologically relevant values used by Braun *et al.* (1998), given in Table I. An example of a single, uncoupled firing neuron for these parameter values is shown in Figure 1.

Global Coupling (Abrams-Strogatz Configuration). Chimera simulations with global coupling are set up as follows. Two groups of 18 identical Huber-Braun neurons are allowed to begin firing. Each neuron is initialized at a random phase within its action potential firing cycle by setting the neuron's initial voltage to a value uniformly and randomly distributed between −75 mV and 0 mV. The coupling term c_i in Eq. (1) is given by

$$c_{i,A} = g_A(V_{i,A}(t) - \bar{V}_A(t-\tau)) + g_{AB}(V_{i,A}(t) - \bar{V}_B(t-\tau)) \tag{10}$$

for neurons in group A, and

$$c_{i,B} = g_B(V_{i,B}(t) - \bar{V}_B(t-\tau)) + g_{AB}(V_{i,B}(t) - \bar{V}_A((t-\tau)) \tag{11}$$

for neurons in group B. Here, the subscript i refers to the particular neuron of interest. $V_{i,A}$ and $V_{i,B}$ denote the instantaneous voltage for neurons in groups A and B, respectively, at time t, and τ is a constant time delay. The terms $\bar{V}_A$ and $\bar{V}_B$ denote the mean voltage of groups A and B, respectively, at some time $t-\tau$. The parameters g_A and g_B represent the coupling strength within each group, and g_{AB} represents the coupling strength between the two groups. Thus, each neuron in a group is coupled to the mean field of its fellow group members, and also, with a different coupling strength, to the mean

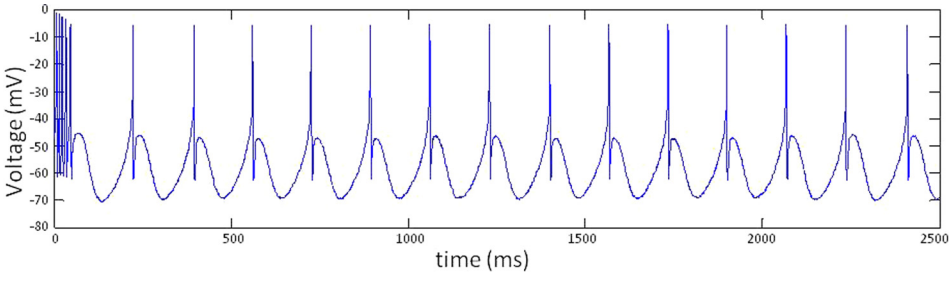

FIG. 1. *Example firing pattern of single uncoupled Huber-Braun neuron.* Example of single Huber-Braun neuron's natural firing pattern when uncoupled with system parameters set as described in Section II.

field of the other group. At the start of each simulation, coupling is "turned on" within group A (thus $g_A \neq 0$), while $g_B = g_{AB} = 0$. After a time interval T_{del}, coupling within group B is activated (with $g_B = g_A$). Simultaneously, coupling is activated between the two groups (with $g_{AB} < g_A, g_B$).

Distance-dependent Coupling (Kuramoto Configuration). In addition to the globally coupled model, we investigated chimera states in a group of Huber-Braun neurons in which the coupling term decayed exponentially with distance. In this case, a ring of N neurons was defined with identical parameters (though starting at different phases of their action potential cycles, as in the global coupling case). For any neuron i, the coupling term in Eq. (1) was given by

$$c_i = \sum_{j \neq i} K'\{V_i(t) - V_j(t-\tau)\}e^{-\kappa x_{ij}}, \tag{12}$$

where the summation is over all the other neurons except the ith. The variable x_{ij} denotes the distance between the ith and the jth neuron, in units of "neurons." Thus, adjacent neurons have $x = 1$, neurons separated by one neighbor have $x = 2$, and so on. The parameter K' defines the amplitude of the coupling term, and the parameter κ defines how quickly the coupling falls off with distance. Simulations were performed for a range of values of K', κ, τ, and N. As with the previous case, chimera states were observed for some values of the system parameters. In this case, however, groups of neurons split off into synchronized or unsynchronized groups spontaneously, rather than being defined *a priori* as groups A and B.

III. RESULTS

Global Coupling (Abrams-Strogatz Configuration). Simulations showed that for certain ranges of the parameters g_A, g_B, g_{AB}, and τ, groups A and B exhibited significantly different behaviors. In some cases, as in the example shown in Figure 2, group A (neurons 1–18) exhibited synchronized behavior, while group B (neurons 19–36) remained unsynchronized, indicating a chimera state. Figure 2(a) shows a raster plot of the neural firing for a portion of the simulation; symbols indicate neural firing times, with the firing times of each neuron indicated in a different row. In this figure and in all subsequent results shown, the firing time is defined by the positive crossing of a $V_m = -20$ mV threshold. Here, $\tau = 58$ ms, and $g_A = 0.013$. For $t < T_{del} = 12\,500$ ms, $g_B = 0$ and $g_{AB} = 0$. For $t \geq T_{del}$ (indicated by the red arrow), $g_B = g_A$ and $g_{AB} = -0.001$. Figure 2(b) shows the mean field of group A (black trace) and the mean field of group B (red trace) over the time interval shown in Figure 2(a), where the mean field is the average V_m of all the neurons in a given group at time t. Note the pairs of spikes visible in the raster plot for both groups A and B, and also clearly visible in the mean field oscillations, indicating a burst-firing pattern of double spikes ("doublets"). The parameter which controls the bifurcation behavior of the Huber-Braun model is the temperature, set at $T = 30°$ C, which results in the firing of single isolated spikes in uncoupled neurons. The values of τ used here are in a physiologically relevant range; the coupling constant values are less physiological and were chosen primarily for their ability to generate chimera states.

Figure 3 illustrates a type of behavior known as a *phase-cluster* state. The simulations shown here are conducted for parameters identical to those shown in Figure 2, except that $g_{AB} = -0.011$. The raster plot in Figure 3(a) shows that group A neurons fire double spikes, while most neurons in group B fire single spikes. This can be seen more clearly in the mean field plots for a short time interval during the simulation, showing group B (red trace, Fig. 3(b)) and group A (black trace, Fig. 3(c)). As can be seen from the raster plots

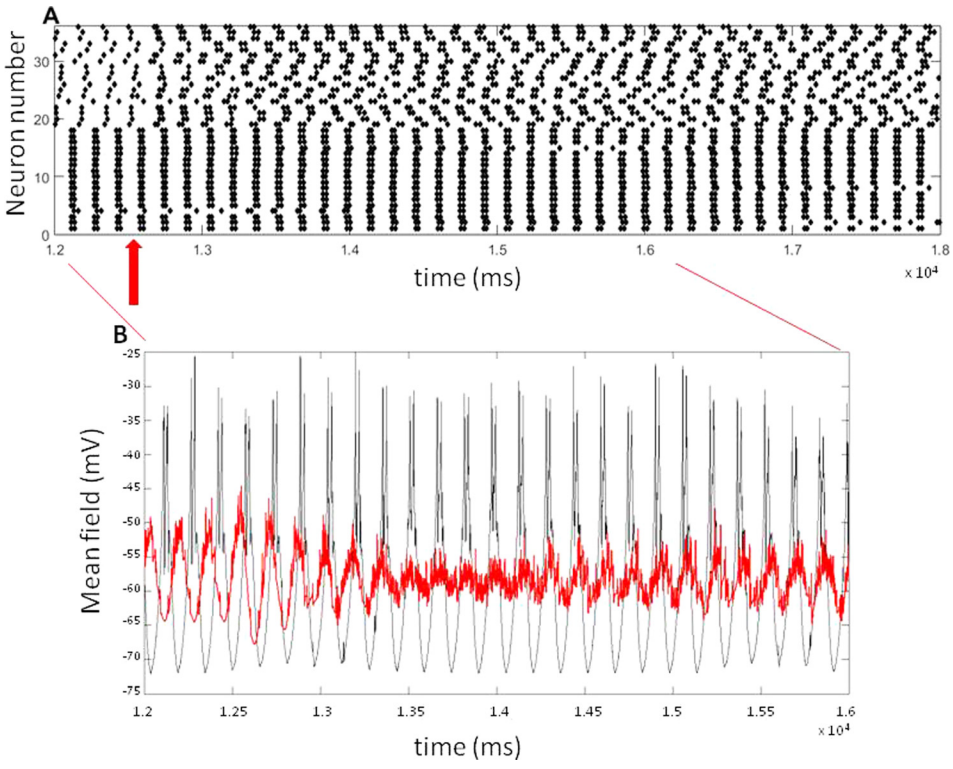

FIG. 2. *Example of a chimera state in the Abrams-Strogatz configuration.* (a) Raster plot illustrating neural spike times during the induction of a chimera state. Neuron number (1–36) is shown on the vertical axis, time is shown on the horizontal axis, and diamonds indicate the firing time of each neuron. The arrow indicates the time at which mean field coupling was initiated among the neurons in group B (19–36), with coupling constant $g_B = g_A = 0.013$, and between groups A and B, with $g_{AB} = -0.001$. The time delay was set at $\tau = 58$ ms. (b) Mean field voltage in group A (black trace) and in group B (red trace) for a subset of the time interval shown in panel (a).

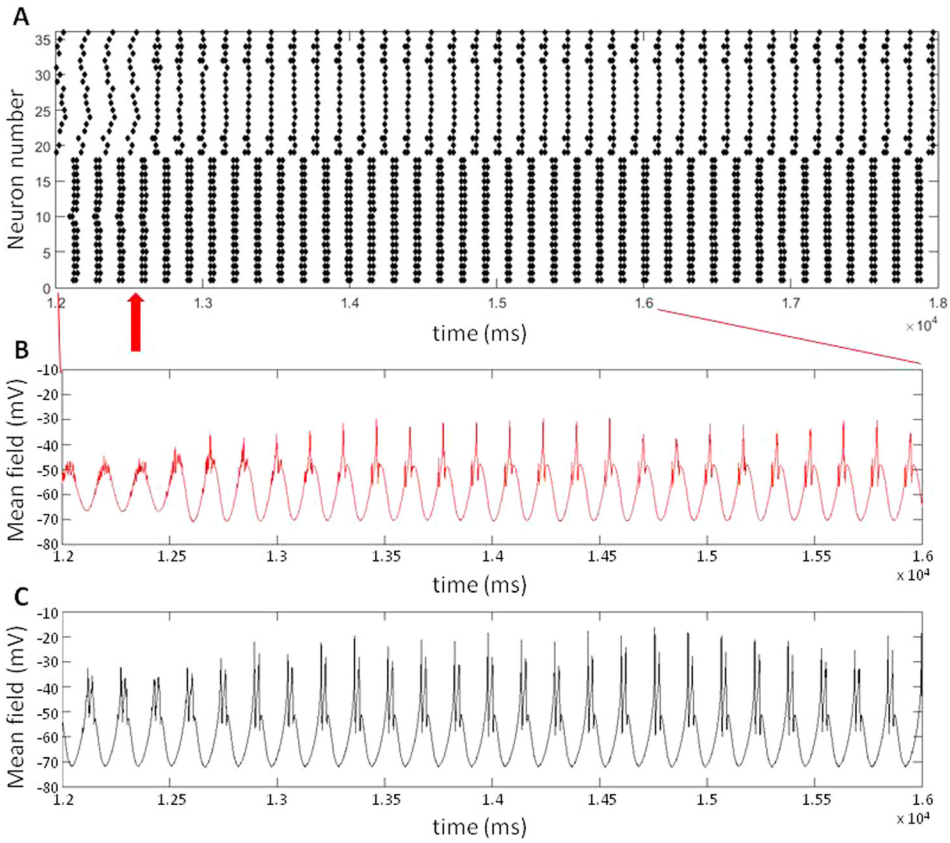

FIG. 3. *Example of a phase-cluster state in the Abrams-Strogatz configuration*. (a) Raster plot; all parameters and conditions are the same as in Figure 2, except that $g_{AB} = -0.011$. (b) Mean field voltage in group B (neurons 19–36) for a subset of the time interval shown in panel (a). (c) Mean field in group A (neurons 1–18) over the same time interval shown for group B.

in Figure 4, the chimera state persists over a longer time interval for $g_{AB} = -0.002$ (Fig. 4(a)) than for the other values of g_{AB} shown. This suggests that the temporal persistence of chimera states may vary with the between-group coupling constant g_{AB}.

In order to quantitatively characterize the chimera states as a function of the control parameters τ and g_{AB}, we determined the stochastic phase synchronization index (Pikovsky *et al.*, 2001) in group A and group B, for $t \geq T_{del}$ for all simulated values of τ and g_{AB}. If neuron i spikes at time t_i and

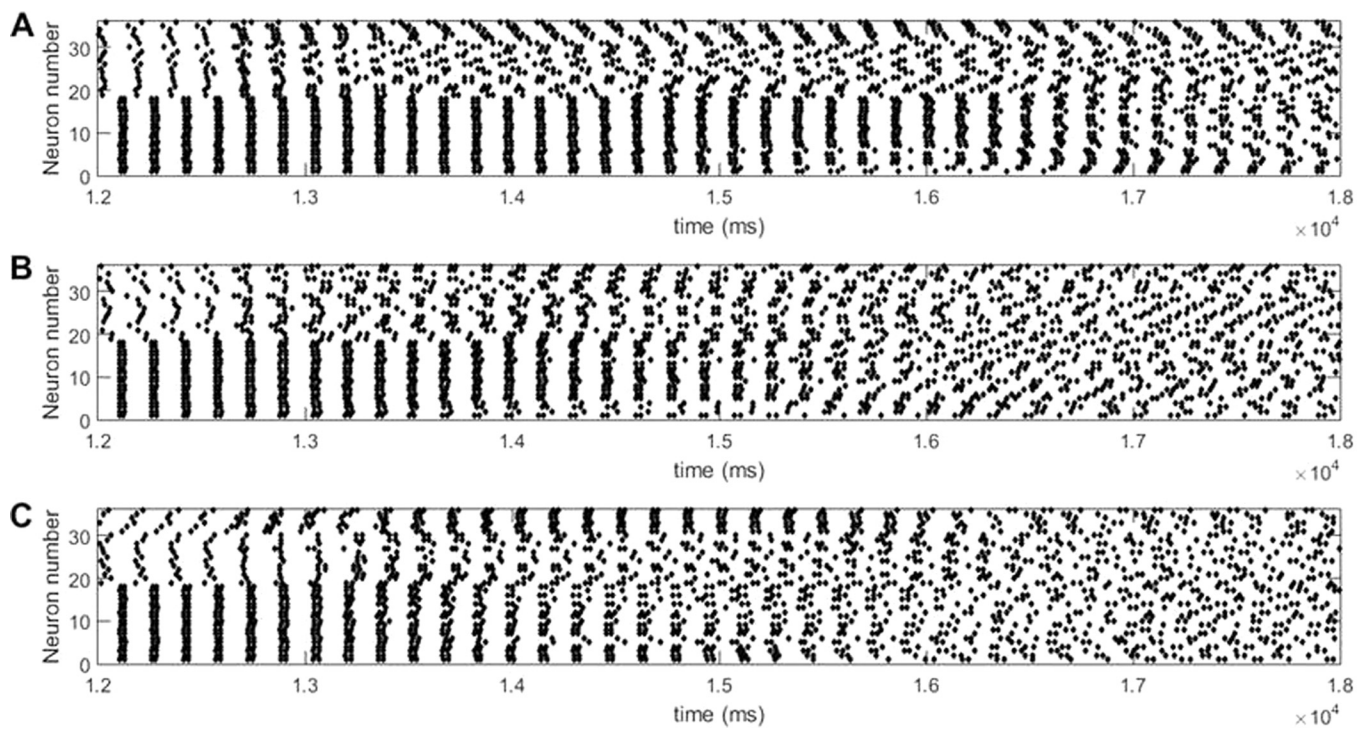

FIG. 4. *Raster plots illustrating temporal variability in the observed chimera states*. Parameters are identical to those for the data shown in Figures 2 and 3, except that in panel (a), $g_{AB} = -0.002$, in panel (b), $g_{AB} = -0.003$, and in panel (c), $g_{AB} = -0.004$.

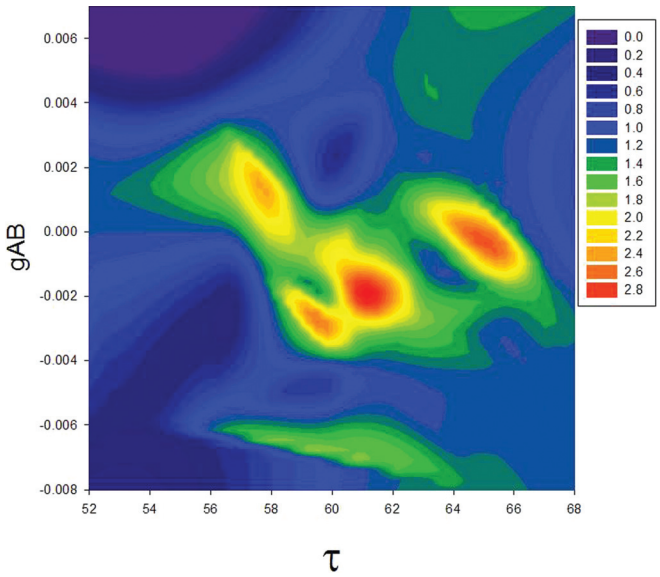

FIG. 5. *Ratio of synchronization indices in group A vs. group B*. Indices are plotted as a function of parameters g_{AB} and τ. Simulations were performed for values of τ ranging from 52 to 68 ms in steps of 1 ms, and with values of g_{AB} ranging from −0.008 to 0.007 in steps of 0.001.

neuron k at times t_k, then, for $t_k < t_i < t_{k+1}$, the phase difference between them is defined as

$$\varphi_{ik}(t_i) = 2\pi(t_i - t_k)/(t_{k+1} - t_k). \tag{13}$$

Neurons (or indeed, any pair of oscillators) exhibit *stochastic phase synchronization* when their phase difference remains relatively constant over a period of time. The degree of synchronization ranges from 0 (completely desynchronized) to 1 (perfectly synchronized) and is quantified by the synchronization index γ_{ik} between neurons i and k, given by

$$\gamma_{ik}^2 = \langle \cos(\varphi_{ik}(t_i)) \rangle^2 + \langle \sin(\varphi_{ik}(t_i)) \rangle^2, \tag{14}$$

where the brackets denote a time average over the interval of interest. The synchronization index, in essence, quantifies the sharpness of the peak of the distribution of phase differences.

For $t \geq T_{del}$, we determine average synchronization indices for groups A and B. The average synchronization index within a group G, containing N neurons, is the average of the synchronization indices between all non-identical pairs of neurons. Thus,

$$\bar{\gamma}_G = \frac{\sum_{i,k} \gamma_{ik}}{N(N-1)/2}. \tag{15}$$

When a chimera state is present, it is expected that the average synchronization index for group A ($\bar{\gamma}_A$) will be high, while group B will have a much lower index ($\bar{\gamma}_B$). Figure 5 shows a parameter space plot of the ratio of these indices

$$\rho = \bar{\gamma}_A / \bar{\gamma}_B. \tag{16}$$

The red end of the color scale corresponds to a high value of this ratio, indicating the presence of a chimera state. (The observation of a phase-cluster state in Figure 3 occurred for parameter values below the bottom edge of the region shown in Figure 5.)

Distance-dependent Coupling (Kuramoto Configuration). Examples of chimera states for exponentially decaying coupling are illustrated in the raster plots shown in Figure 6. Figure 6(a), for $K' = 0.010$, $\kappa = 1.10$, $N = 54$, and $\tau = 48$ ms, shows initial synchrony in the entire ring, after which unsynchronized clusters emerge. These grow in size, eventually taking over a large proportion of the entire population. A small group of synchronized neurons remain, though the synchronized behavior drifts through the population. In Figure 6(b), for $K' = 0.011$, $\kappa = 1.10$, $N = 54$, and $\tau = 48$ ms, we see the emergence of a single large unsynchronized cluster within the initially synchronized population. The synchronized behavior is squeezed into a smaller population, but new synchronized subpopulations emerge for $t > 14\,000$ ms.

One parameter held constant in all the results shown above is the amplitude of the noise term. Preliminary simulations varying the noise amplitude while holding all other parameters constant suggest that, for values of K', κ, and τ which yield chimera states, the chimera behavior is relatively robust with respect to the noise amplitude. Larger noise amplitudes appear to disrupt the chimera state and yield asynchronous activity within the entire population (data not shown). Decreasing the noise amplitude appears to have some effect on the lifetime of the chimera state, though this remains to be explored in more detail in further studies. Note

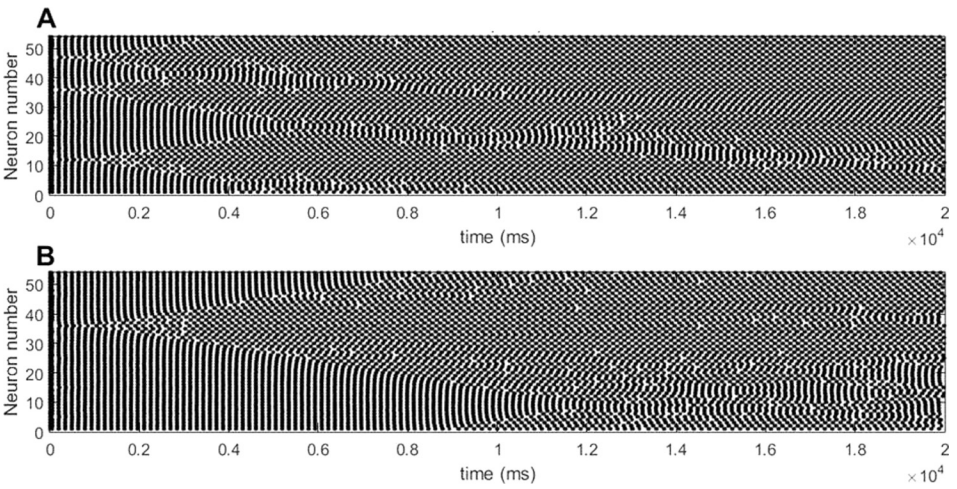

FIG. 6. *Chimera states in the Kuramoto configuration.* (a) Raster plot of neural firing times for a circular configuration of 54 coupled Huber-Braun neurons, with $K' = 0.010$, $\kappa = 1.10$, and $\tau = 48$ ms. Note the emergence of desynchronized clusters. (b) Simulation under identical conditions to panel (a), but with $K' = 0.011$.

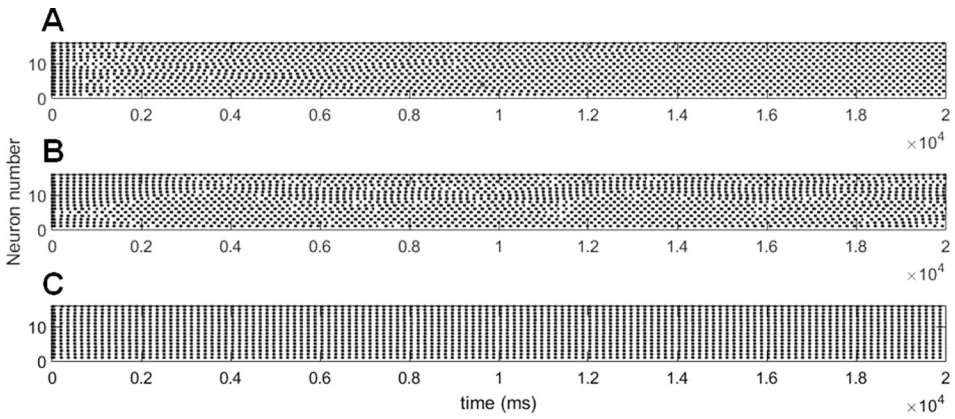

FIG. 7. *Chimera and fully synchronized states in the Kuramoto configuration.* Raster plots of firing times of a circular configuration of 16 coupled Huber-Braun neurons, with $K' = 0.011$ and $\kappa = 1.10$. (a) $\tau = 38$ ms; (b) $\tau = 48$ ms; and (c) $\tau = 58$ ms.

that due to the presence of noise in the system, the behavior of the different populations must be assessed using a stochastic phase synchronization measure; as a result, *complete* synchronization such as that found in "classical" chimeras described by Kuramoto and Battogtokh (2002) or by Abrams *et al.* (2008) will not be observed here.

As expected, the existence of chimera states is highly dependent on the system parameters. Figure 7 shows three simulations, each with $K' = 0.011$, $\kappa = 1.10$, and $N = 18$. With a time delay of $\tau = 38$ ms (Fig. 7(a)), the neurons exhibit anti-phase firing. For $\tau = 48$ ms (Fig. 7(b)), chimera behavior is observed, and drifting groups of synchronized and unsynchronized neurons persist for the duration of the simulation. For $\tau = 58$ ms (Fig. 7(c)), the entire system exhibits in-phase synchronous activity.

The behavior of the system is characterized in parameter space, for $\tau = 58$ ms, in Figure 8. In both panels, K' was varied from 0.001 to 0.033 in increments of 0.001, and κ was varied from 1.0 to 2.0 in increments of 0.01. The color scale represents the fraction of neuron pairs (out of a total of 153 unique pairs) that had a synchronization index of 0.6 or greater. Red areas (1.0) signify that 153 of 153 pairs of neurons were synchronized, which represents a fully synchronized state. Purple areas (0.0), conversely, signify a complete desynchronization of all neuron pairs. Figure 8(a) shows synchronization during the first half of the simulation, and Figure 8(b) shows results from the second half. The total simulation was carried out over 500 000 time steps in increments of 0.01 ms. An initial 50 time steps were discarded as transients, and the remaining time interval was split into two segments of equal duration. Note that the boundaries between regions of synchronization and desynchronization become more sharply delineated in the second half of the simulation (Fig. 8(b)).

Figure 8 shows distinct bands (labeled I to IV) of synchronization, separated by bands of desynchronization. Furthermore, the neural firing pattern changes from region to region, as illustrated in Figure 9. The panels in Figure 9 show raster plots of neural firing in regions I through IV in Figure 8, for parameter values marked by the four-pointed stars in Figure 8(a). For $\kappa = 1.04$ and $K' = 0.001$, all neurons in the system fire single spikes (Fig. 9(a)); for $K' = 0.010$, the system fires synchronized doublets (Fig. 9(b)); for $K' = 0.022$, synchronized triplets (Fig. 9(c)); and for $K' = 0.030$, synchronized quadruplets (Fig. 9(d)).

Chimera states would be expected to occur at the boundary between synchronized and desynchronized regions since, in a chimera state, a portion of the neural population would exhibit synchrony, while the remainder of the neurons would be desynchronized, leading to an intermediate overall value of the synchronization index. This is indeed observed, as shown in Figure 10. Here, panels correspond to the parameter values marked with

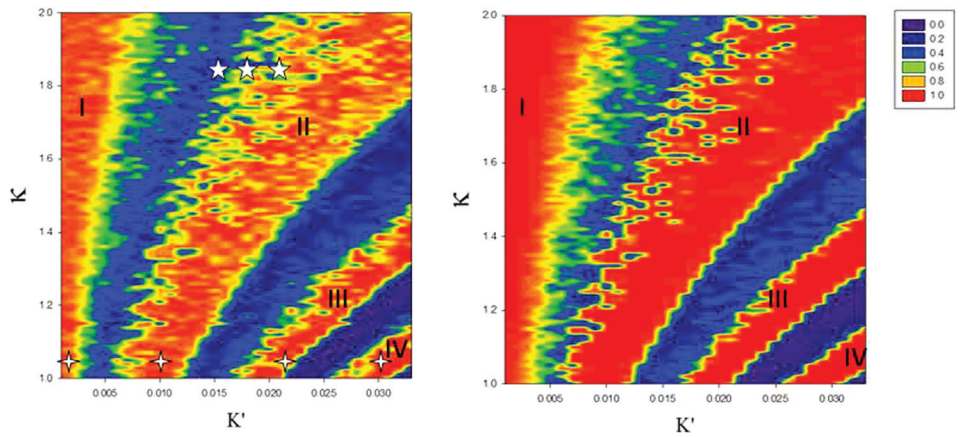

FIG. 8. *Contour plot of synchronization ratios for Kuramoto configuration.* The ratios of unique synchronized pairs of neurons to the total number of unique neural pairs are shown for the first half (a) and for the second half (b) of the simulation time course, over a range of parameter values. Color scale indicates the ratio of unique synchronized neural pairs with synchronization index of 0.6 or greater to the total number of unique neural pairs. Values of κ run from 1.0 to 2.0 in increments of 0.01, and values of K' run from 0.001 to 0.033 in increments of 0.001. τ was set at 58 ms.

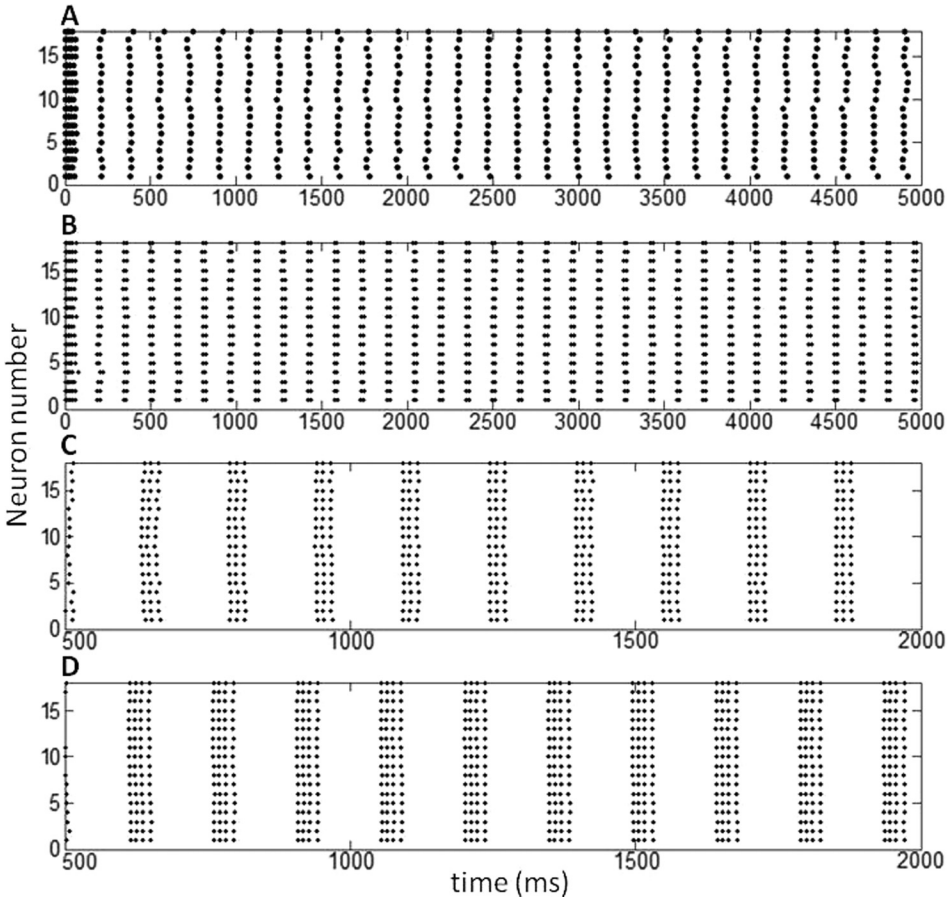

FIG. 9. *Synchronized bursting behavior in the Kuramoto configuration.* Panels show raster plots of spike times for parameter values corresponding to the four-pointed stars in Figure 8(a). For all panels, $\kappa = 1.04$. Values of K' are (a) 0.001, (b) 0.010, (c) 0.022, and (d) 0.030.

five-pointed stars in Figure 8(a), illustrating transient chimera states for $\kappa = 1.85$, with $K' = 0.013$ (Fig. 10(a)), $K' = 0.017$ (Fig. 10(b)), and $K' = 0.018$ (Fig. 10(c)).

IV. DISCUSSION AND CONCLUSIONS

We have demonstrated chimera states and phase-cluster states in the Huber-Braun neural model, a realistic Hodgkin-Huxley-type model designed to simulate the activity of mammalian facial cold receptors. These behaviors occur both in the case of global mean-field coupling between two identical groups of neurons (Abrams-Strogatz coupling) and in the case of distance-dependent coupling (Kuramoto coupling). In each case, the system's behavior has been characterized over a range of parameter values, using the stochastic phase synchronization index. In some cases of Kuramoto

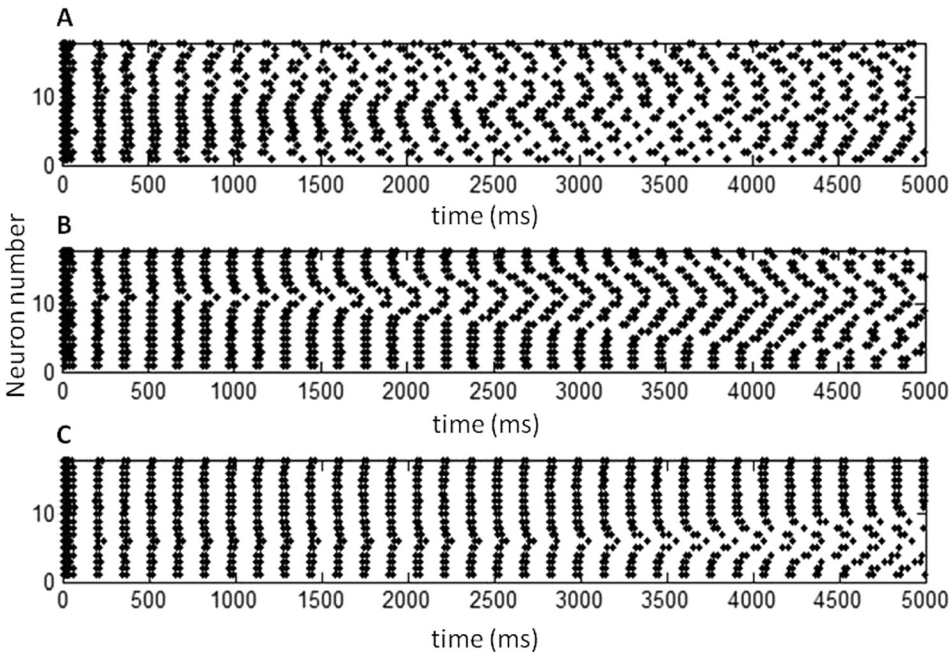

FIG. 10. *Transient chimera states in the Kuramoto configuration.* Panels show raster plots of spike times for parameter values corresponding to the five-pointed stars in Figure 8(a). For all panels, $\kappa = 1.85$. Values of K' are (a) 0.013, (b) 0.017, and (c) 0.018.

coupling, such as that shown in Figure 7, we observe chimera states in which a synchronized cluster of oscillators wanders irregularly around the ring, reminiscent of the results observed by Sethia *et al*. (2013) in their study of chimera state solutions of the complex Ginzburg-Landau equation. Our results also resemble the Brownian motion-like drifting of coherent and incoherent regions discussed by Omel'chenko *et al*. (2010) using a ring of phase oscillators. In other cases, such as those shown in Figures 4(b) and 4(c) with Abrams-Strogatz coupling, we observe a collapse of the chimera state, as discussed by Wolfrum and Omel'chenko (2011).

The parameters used here result only in single-spiking behavior in *uncoupled* neurons. However, we observe the onset of bursting behavior when the neurons are coupled. Phase-cluster states, for example, can consist of a group of synchronized neurons firing single spikes and a group of synchronized neurons exhibiting burst-firing, as shown in Figure 3 for Abrams-Strogatz coupling. Coupling-induced bursting is also observed in the Kuramoto configuration, in the bands of synchronized behavior shown in Figures 8 and 9. Here, for a constant value of κ, the system passes through alternating regimes of synchronization and desynchronization as the coupling amplitude K' is varied. In each successive band of synchronized behavior, the system exhibits an additional spike per burst, moving from single spikes (region I, Fig. 9(a)) to doublets (region II, Fig. 9(b)), to triplets (region III, Fig. 9(c)), and finally to quadruplets (region IV, Fig. 9(d)). The observations of coupling-induced bursting are consistent with the previous observations of increased bursting behavior in coupled Huber-Braun neurons; an increased number of spikes per burst occurs in this system as the coupling constant is increased (Bahar, 2004 and Weihberger and Bahar, 2007). As the control parameter T is decreased in uncoupled Huber-Braun neurons, the system exhibits a period-adding bifurcation cascade; holding T constant while sweeping the coupling constant amplitude has the effect, in essence, of recapitulating this bifurcation pattern.

In addition to the bursting patterns contained within the different bands shown in Figure 8, several other aspects of this parameter space representation deserve comment. First to note is the sharpening of the synchronized regions during the second half of the simulations (Fig. 8(b)). This suggests the decay of transient behavior over time, producing more clearly defined boundaries between synchronized and desynchronized states. This also narrows the regions of parameter space where chimera states live, consistent with the idea that chimeras may be chaotic transients (Wolfrum and Omel'chenko, 2011).

The lower boundary of each synchronized region shows a sawtooth pattern; this is simply a result of the step size by which K' was varied between simulations. More interesting is the observation that the synchronization-desynchronization boundary is more diffuse on the left-hand side of each synchronization region. This may result from the fact that, along the left boundary, not only is K' smaller, resulting in a weaker overall coupling, but also κ is larger, yielding a faster exponential decay of the coupling term with distance. The complex structure of these synchronization-desynchronization boundaries is retained even in the second half of the simulations, as shown in Figure 8(b). It is possible that a fractal basin boundary exists between these regions; this could be investigated by using a finer grid of parameter values.

The results shown in Figure 8 exhibit common features with the results of Omel'chenko, Maistrenko, and Tass (2008), who identified chimera states in a network of globally coupled oscillators with spatially modulated delayed feedback. Their results demonstrated that chimera states could emerge in systems for a wide range of initial conditions, rather than having to be approached via a specific set of initial conditions, as necessary in the case where a chimera state is simultaneously stable with a stable coherent state. They characterized chimera states as forming a "natural link between coherence and incoherence," showing chimera states existing at the boundaries between regions of coherence and incoherence in parameter space. This is precisely what is observed in our system, with chimera states existing at the boundaries of Arnol'd-tongue-like regions; note the similarity in structure between our Figure 8 and Figure 3 in Omel'chenko, Maistrenko, and Tass (2008).

We observe the transient formation and dissipation of synchronized clusters in the case of Kuramoto coupling, and occasionally with Abrams-Strogatz coupling as well. The persistence of transient synchronized clusters appears to be influenced by system parameters such as coupling constants (Fig. 4) and time delay (Fig. 7). We have not observed relaxation of the system to a statistically stationary state; it is possible, however, that simulations performed for significantly longer time intervals may reveal such behavior.

Given their obvious interest for the modeling of neural processes involving synchronization, chimera states have been investigated previously in simpler neural models than that used here. Olmi *et al*. (2010) observed chimera states in a one-variable leaky integrate-and-fire model. In contrast to the exponentially decaying coupling used in the present work for the Kuramoto coupling case, Omelchenko *et al*. (2013) used a constant nonzero coupling strength σ within a coupling radius r, and set the coupling constant to zero beyond this radius. That study, like the present paper, incorporates the biological observation that, at least in neocortical tissue, the majority of neural connections are local. Our study, however, allows for weak long-range connections extending through the entire network. Omelchenko *et al*. (2013) also showed the emergence of *multichimera states* in their system for stronger coupling constants. In a multichimera state, several regions of incoherent activity exist within the system, separated by regions of coherence. We observe such multichimera states in our system as well, as illustrated in Figure 6(a). Future work will investigate the dependence of such states on system parameters such as the coupling strength.

In 2014, Hizanidis and colleagues investigated chimera states in the Hindmarsh-Rose model, which in its three-dimensional formulation includes a slow variable that allows for bursting behavior. Using a coupling scheme similar to that of Omelchenko *et al*. (2013), Hizanidis *et al*. (2014) demonstrated chimera behavior including multichimera states. They also observed *mixed oscillatory states*, in which

desynchronized oscillators were interspersed among synchronized ones. We observe something reminiscent of this in the "phase cluster" state shown in Figure 3(a). Here, one group of neurons exhibits doublet firing; the other group fires single spikes, except for a few oscillators within this group that fire doublets.

A chimera model in a small group of neurons is only a simple proxy for the complexity of an actual brain, with its many types of neurons and glia, its mixture of local and long-range connectivity, and its synaptic plasticity. Nonetheless, neural chimera models may provide a starting point for modeling phenomena such as unihemispheric sleep in various species. Without scaling up to much larger simulations, chimera models can merely provide a schematic guide to the underlying processes that drive whole-brain phenomena such as unihemispheric sleep. A computational model for unihemispheric sleep was recently proposed by Kedziora *et al*. (2012), who found unihemispheric sleep to be favored by inhibitory coupling between the brain hemispheres. This is reminiscent of our finding that chimera states are more prevalent for negative coupling constants in the Abrams-Strogatz case (our Figure 5; see also Figure 2(a) in Tinsley *et al*., 2012).

Neural chimera models may also provide insight into other problems in neurodynamics in which different subsystems exhibit transient, dynamical decoupling without the actual severance of synaptic connections. Given the range of *in vitro* neural synchronization studies performed in recent years (Feldt *et al*., 2010; Chen and Dzakpasu, 2010; and Niedringhaus *et al*., 2015), it is likely that proof-of-concept neural chimeras studies can be performed in cultured neural systems, providing insights into conditions under which neural chimera states are most likely to occur.

Future studies of transient neural chimera states may provide insights into role played by the dynamical reorganization of brain networks in cognition (Bola and Sabel, 2015 and Voytek and Knight, 2015). Battaglia *et al*. (2012) proposed "on-demand reconfiguration" of neural circuits was proposed as a mechanism of information processing. Recent fMRI studies have suggested that dynamic reconfiguration of networks in the frontal cortex may play a role in executive cognition in human subjects (Braun *et al*., 2015). The formation and dissolution of chimera states might well provide a substrate for such transient dynamics. Chimera states may also be relevant to models of working memory and visual orientation tuning due to their similarity to "bump states" (Laing and Chow, 2001; Laing, 2015; and Panaggio and Abrams, 2015), which have been suggested as models of these forms of cortical information processing. Bump states occur when a group of asynchronously firing neurons persists within a network that otherwise exists in an "off" state (Laing, 2001), or when a partially synchronous neural cluster occurs embedded within a larger group of asynchronously firing neurons (Laing, 2011). Like synchronized or desynchronized clusters in a chimera state, bumps have been shown to wander through a network of spiking neurons (Chow and Coombes, 2006).

In order to adapt neural chimera models to aid in modeling processes that can be characterized by bump states, such as working memory, it will likely be necessary to employ models with a heterogeneous neural population. Laing (2009a and 2009b) showed that chimera states can exist in networks of neurons with a heterogeneous distribution of frequencies, though their stability depends on the width of the frequency distribution and, in the case of Abrams-Strogatz coupling, on whether one or both of the groups have a heterogeneous frequency distribution. The Huber-Braun model lends itself easily to such investigations, though in the context of modeling cognitive processes, a neural model such as that designed by Wilson (1999), which specifically models mammalian neocortical neurons and allows for a variety of realistic firing patterns, might be more appropriate.

ACKNOWLEDGMENTS

The authors thank Shane Meyer for useful discussions regarding the interpretation of Figure 8. We also thank Professor Kenneth Showalter for inspiration and useful discussions and thank the anonymous referees for their useful comments and suggestions, which have greatly strengthened the paper.

Abeyratne, U. R., Swarnkar, V., Hukins, C., and Duce, B., "Interhemispheric asynchrony correlates with severity of respiratory disturbance index in patients with sleep apnea," IEEE Trans. Biomed. Eng. **57**, 2947–2955 (2010).

Abrams, D. M., Mirollo, R., Strogatz, S. H., and Wiley, D. A., "Solvable model for Chimera states of coupled oscillators," Phys. Rev. Lett. **101**, 084103 (2008).

Abrams, D. M. and Strogatz, S. H., "Chimera states for coupled oscillators," Phys. Rev. Lett. **93**(17), 174102 (2004).

Adamchic, I., Hauptmann, C., Barnikol, U. B., Pawelczyk, N., Popovych, O., Barnikol, T. T., Silchenko, A., Volkmann, J., Deuschl, G., Meissner, W. G., Maarouf, M., Sturm, V., Freund, H. J., and Tass, P. A., "Coordinated reset neuromodulation for Parkinson's disease: Proof-of-concept study," Mov. Disord. **29**(13), 1679–1684 (2014).

Bahar, S., "Burst-enhanced synchronization in an array of noisy coupled neurons," Fluctuation Noise Lett. **4**(1), L87–L96 (2004).

Bartolomei, F., Guye, M. F., and Wendling, F., "Abnormal binding and disruption in large scale networks involved in human partial seizures," EPJ Nonlinear Biomed. Phys. **1**, 4 (2013).

Battaglia, D., Witt, A., Wolf, F., and Geisel, T., "Dynamic effective connectivity of inter-areal brain circuits," PLoS Comput. Biol. **8**(3), e1002438 (2012).

Bola, M. and Sabel, B. A., "Dynamic reorganization of brain functional networks during cognition," Neuroimage **114**, 398–413 (2015).

Braun, W., Eckhardt, B., Braun, H. A., and Huber, M. T., "Phase-space structure of a thermoreceptor," Phys. Rev. E **62**, 6352–6360 (2000).

Braun, H. A., Huber, M. T., Dewald, M., Schäfer, K., and Voigt, K., "Computer simulations of neuronal signal transduction: The role of nonlinear dynamics and noise," Int. J. Bifurcation Chaos Appl. Sci. Eng. **8**(5), 881–889 (1998).

Braun, U., Schäfer, A., Walter, H., Erk, S., Romanczuk-Seiferth, N., Haddad, L., Schweiger, J. I., Grimm, O., Heinz, A., Tost, H., Meyer-Lindenberg, A., and Bassett, D. S., "Dynamic reconfiguration of frontal brain networks during executive cognition in humans," Proc. Natl. Acad. Sci. U. S. A. **112**(37), 11678–11683 (2015).

Chen, X. and Dzakpasu, R., "Observed network dynamics from altering the balance between excitatory and inhibitory neurons in cultured networks," Phys. Rev. E **82**(3 Pt 1), 031907 (2010).

Chow, C. C. and Coombes, S. "Existence and wandering of bumps in a spiking neural network model," SIAM J. Appl. Dyn. Syst. **5**, 552–574 (2006).

Feldt, S., Wang, J. X., Shtrahman, E., Dzakpasu, R., Olariu, E., and Zochowski, M., "Functional clustering in hippocampal cultures: Relating network structure and dynamics," Phys. Biol. **7**(4), 046004 (2010).

Feudel, U., Neiman, A., Pei, X., Wojtenek, W., Braun, H., Huber, M., and Moss, F., "Homoclinic bifurcation in a Hodgkin-Huxley model of thermally sensitive neurons," Chaos **10**(1), 231–239 (2000).

Fox, R. F., Gatland, I. R., Roy, R., and Vemuri, G., "Fast, accurate algorithm for numerical simulation of exponentially correlated colored noise," Phys. Rev. A **38**, 5938–5940 (1988).
Fries, P., Reynolds, J. H., Rorie, A. E., and Desimone, R., "Modulation of oscillatory neuronal synchronization by selective visual attention," Science **291**(5508), 1560–1563 (2001).
Hagerstrom, A. M., Murphy, T. E., Roy, R., Hövel, P., Omelchenko, I., and Schöll, E., "Experimental observation of chimeras in coupled-map lattices," Nat. Phys. **8**, 658–661 (2012).
Hizanidis, J., Kanas, V. G., Bezerianos, A., and Bountis, T., "Chimera states in networks of nonlocally coupled Hindmarsh-Rose neuron models," Int. J. Bifurcation Chaos Appl. Sci. Eng. **24**(3), 1450030 (2014).
Huber, M. T., Krieg, J. C., Dewald, M., Voigt, K., and Braun, H. A., "Stochastic encoding in sensory neurons: impulse patterns of mammalian cold receptors," Chaos, Solitons Fractals **11**, 1895–1903 (2000).
Isomura, Y., Fujiwara-Tsukamoto, Y., and Takada, M., "A network mechanism underlying hippocampal seizure-like synchronous oscillations," Neurosci. Res. **61**(3), 227–33 (2008).
Kedziora, D. J., Abeysuriya, R. G., Phillips, A. J. K., and Robinson, P. A., "Physiologically based quantitative modeling of unihemispheric sleep," J. Theor. Biol. **314**, 109–119 (2012).
Kuramoto, Y. and Battogtokh, D., "Coexistence of coherence and incoherence in nonlocally coupled phase oscillators," Nonlinear Phenom. Complex Syst. **5**, 380–385 (2002); available at http://www.j-npcs.org/online/vol2002/v5no4/v5no4p380.pdf.
Laing, C. R., "Chimera states in heterogeneous networks," Chaos **19**, 013113 (2009a).
Laing, C. R., "The dynamics of chimera states in heterogeneous Kuramoto networks," Physica D **238**, 1569–1588 (2009b).
Laing, C. R., "Fronts and bumps in spatially extended Kuramoto networks," Physica D **240**, 1960–1971 (2011).
Laing, C. R., "Exact neural fields incorporating gap junctions," SIAM J. Appl. Dyn. Syst. **14**, 1899–1929 (2015).
Laing, C. R. and Chow, C. C., "Stationary bumps in networks of spiking neurons," Neural Comput. **13**, 1473–1494 (2001).
Lyamin, O. I., Manger, P. R., Ridgway, S. H., Mukhametov, L. M., and Siegel, J. M., "Cetacean sleep: An unusual form of mammalian sleep," Neurosci. Biobehav. Rev. **32**, 1451–1484 (2008).
Martens, E. A., Thutupalli, S., Fourrière, A., and Hallatschek, O., "Chimera states in mechanical oscillator networks," Proc. Natl. Acad. Sci. U. S. A. **110**(26), 10563–10567 (2013).
Mathews, C. G., Lesku, J. A., Lima, S. L., and Amlaner, C. J., "Asynchronous eye closure as an anti-predator behavior in the western fence lizard (*Sceloporus occidentalis*)," Ethology **112**, 286–292 (2006).
Mukhametov, L. M., in *Sleep Mechanisms*, edited by Borbely, A. and Valatx, J. L. (Springer Verlag, 1984), pp. 227–238.
Niedringhaus, M., Chen, X., and Dzakpasu, R., "Long-term dynamical constraints on pharmacologically evoked potentiation imply activity conservation within *in vitro* hippocampal networks," PLoS One **10**(6), e0129324 (2015).
Nkomo, S., Tinsley, M. R., and Showalter, K., "Chimera states in populations of nonlocally coupled chemical oscillators," Phys. Rev. Lett. **110**, 244102 (2013).
Olmi, S., Politi, A., and Torcini, A., "Collective chaos in pulse-coupled neural networks," Europhys. Lett. **92**, 60007 (2010).
Omel'chenko, O. E., Maistrenko, Y. L., and Tass, P. A., "Chimera states: the natural link between coherence and incoherence," Phys. Rev. Lett. **100**, 044105 (2008).
Omelchenko, I., Omel'chenko, O. E., Hövel, P., and Schöll, E., "When nonlocal coupling between oscillators becomes stronger: Patched synchrony or multichimera states," Phys. Rev. Lett. **110**, 224101 (2013).
Omel'chenko, O. E., Wolfrum, M., and Maistrenko, Y. L., "Chimera states as chaotic spatiotemporal patterns," Phys. Rev. E **81**, 065201(R) (2010).
Panaggio, M. J. and Abrams, D. M., "Chimera states: coexistence of coherence and incoherence in networks of coupled oscillators," Nonlinearity **28**, R67–R87 (2015).
Pikovsky, A., Rosenblum, M., and Kurths, J., *Synchronization: A Universal Concept in Nonlinear Sciences* (Cambridge University Press, Cambridge, 2001).
Popovych, O. V., Hauptmann, C., and Tass, P. A., "Effective desynchronization by nonlinear delayed feedback," Phys. Rev. Lett. **94**(16), 164102 (2005).
Rattenborg, N. C., "Do birds sleep in flight?," Naturwissenschaften **93**, 413–425 (2006).
Rattenborg, N. C., Lima, S. L., and Amlaner, C. J., "Half-awake to the risk of predation," Nature **397**, 397–398 (1999).
Rial, R., González, J., Gené, L., Akaârir, M., Esteban, S., Gamundí, A., Barceló, P., and Nicolau, C., "Asymmetric sleep in apneic human patients," Am. J. Physiol.: Regul., Integr. Comp. Physiol. **304**, R232–R237 (2013).
Sethia, G. C., Sen, A., and Johnston, G. L., "Amplitude-mediated chimera states," Phys. Rev. E **88**, 042917 (2013).
Tamaki, M., Bang, J. W., Watanabe, T., and Sasaki, Y., "Night watch in one brain hemisphere during sleep associated with first-night effect in humans," Curr. Biol. **26**, 1190–1194 (2016).
Tass, P. A., Qin, L., Hauptmann, C., Dovero, S., Bezard, E., Boraud, T., and Meissner, W. G., "Coordinated reset has sustained aftereffects in Parkinsonian monkeys," Ann. Neurol. **72**(5), 816–820 (2012).
Tinsley, M. R., Nkomo, S., and Showalter, K., "Chimera and phase-cluster states in populations of coupled chemical oscillators," Nat. Phys. **8**, 662–665 (2012).
Tononi, G. and Koch, C., "The neural correlates of consciousness: An update," Ann. N. Y. Acad. Sci. **1124**, 239–261 (2008).
Voytek, B. and Knight, R. T., "Dynamic network communication as a unifying neural basis for cognition, development, aging, and disease," Biol. Psychiatry **77**(12), 1089–1097 (2015).
Weihberger, O. and Bahar, S., "Frustration, drift, and antiphase coupling in a neural array," Phys. Rev. E **76**, 011910 (2007).
Wickramasinghe, M. and Kiss, I. Z., "Spatially organized dynamical states in chemical oscillator networks: Synchronization, dynamical differentiation, and chimera patterns," PLoS One **8**(11), e80586 (2013).
Wilson, H. R., "Simplified dynamics of human and mammalian neocortical neurons," J. Theor. Biol. **200**(4), 375–388 (1999).
Wolfrum, M. and Omel'chenko, O. E., "Chimera states are chaotic transients," Phys. Rev. E **84**, 015201(R) (2011).